JOURNAL OF GUIDANCE, CONTROL, AND DYNAMICS
Vol. 31, No. 3, May–June 2008

Invariant Manifolds and Orbit Control in the Solar Sail Three-Body Problem

Thomas J. Waters* and Colin R. McInnes†
University of Strathclyde, Glasgow, Scotland G1 1XJ, United Kingdom

DOI: 10.2514/1.32292

In this paper, we consider issues regarding the control and orbit transfer of solar sails in the circular restricted Earth–sun system. Fixed points for solar sails in this system have the linear dynamic properties of saddles crossed with centers; thus, the fixed points are dynamically unstable and control is required. A natural mechanism of control presents itself: variations in the sail's orientation. We describe an optimal controller to control the sail onto fixed points and periodic orbits about fixed points. We find this controller to be *very* robust, and we define sets of initial data using spherical coordinates to get a sense of the domain of controllability; we also perform a series of tests for control onto periodic orbits. We then present some mission strategies involving transfers from the Earth to fixed points and onto periodic orbits and involving controlled heteroclinic transfers between fixed points on opposite sides of the Earth. Finally, we present some novel methods for finding periodic orbits in circumstances in which traditional methods break down, based on considerations of the center manifold theorem.

I. Introduction

THE notion of a solar sail as a practical and flexible space propulsion option is gathering momentum, and there are a number of proposed missions using the special properties of solar sails. Two examples of such are the exploration of the far solar system (see, for example, Dachwald [1]) and the GeoSail concept (see, for example, McInnes et al. [2]). This enthusiasm is partly due to advances in materials science, making construction of the sails feasible, and partly due to the emerging understanding of the full dynamic possibilities of solar sails. In particular, the solar sail in the setting of the circular restricted three-body problem (CR3BP) has produced new and interesting families of orbits that are beyond the capabilities of conventional spacecraft. This is seen most readily in the fixed points: the classical CR3BP has five isolated fixed points, the Lagrange points, whereas the solar sail CR3BP has a three-parameter family of fixed points. It is this additional freedom due to the sail parameters that makes the solar sail CR3BP such an interesting generalization of the three-body problem. This paper seeks to further extend our understanding of solar sails in the CR3BP by considering the issues of controlling the sail's position or orbit and transferring the sail between fixed points, periodic orbits, and the Earth itself.

The linear stability properties of solar sails in the CR3BP were first examined by McInnes et al. [3] and McInnes [4], and the nature of the fixed points and the linear stability of same were discussed. It was found that there are continuous surfaces of fixed or equilibrium points, and that these points are linearly unstable; we next give a brief recap of the important features of this analysis. The fact that fixed points in the x–z plane have center eigenvalues after linearization can be used to describe (unstable) periodic orbits about the fixed point, and the authors [5] have used the LP method to find families of periodic orbits about fixed points high above the ecliptic plane. In [5], an application of such periodic orbits was suggested for Earth observation: a large-amplitude orbit with a period of one year would counter the effects of the variation in the Earth's axis of rotation when viewed from the poles. Baoyin and McInnes [6] showed how periodic orbits about fixed points on the x axis may also be described. However, the instability inherent in these points and orbits means that a controller must be used to maintain these states over long times.

The natural mechanism of control for a solar sail is in variations of the sail's orientation, and McInnes [7] and Lawrence and Piggott [8] presented some preliminary investigations of the robustness of this control mechanism in the CR3BP. Baoyin and McInnes [9] considered control in the elliptical three-body problem, and Bookless and McInnes [10] and McInnes [11] examined control of solar sails in two-body problems. Also, Gómez et. al. [12] used solar radiation when examining control in the classical CR3BP. In this paper, we will describe an optimal controller that minimizes a cost function, the gains being found from solutions of the algebraic Ricatti equation. This approach is very well known and is used broadly in the literature, and we refer the reader to, for example, Ogata [13]. We consider the efficacy of this controller for fixed points and periodic orbits in Secs. III and IV, respectively. There, we present a number of tests to determine the relative controllability of different points and orbits, to answer questions such as, From which direction of displacement from the fixed point is it hardest to control? How large an orbit may we control onto directly from the fixed point? Which fixed points have the largest domain of controllability?

As we shall see, there is a very large set of fixed points and periodic orbits, and presenting the controllability of each would be tedious and distract from the overall behavior. Instead, when appropriate, we will consider nominal parameter values for which a fixed point in the x–z plane is specified by the parameters β and γ, where β is the sail lightness number and γ is the angle the sail normal makes with the x axis (more detail follows). As nominal β and γ values, we will choose $\beta = 0.05174$ for the following reasons:

1) This is a very moderate value within the feasibility of near-future technology, placing the application of this analysis very much in the near term.

2) This parameter value displays all the relevant features and is thus a representative value.

3) This precise value was used in [5], along with a γ value of 0.8092 rad, to describe orbits of a period of one year and some applications of the same.

In Sec. V, we examine a possible mission made up of different legs, each requiring its own control scheme. This mission consists of transferring from the Earth's vicinity to a high-altitude fixed point, transferring from this point onto a periodic orbit, and the controlled transfer from a fixed point on the L_1 side of the Earth to one on the L_2 side. These transfers combine the control strategy outlined

Received 22 May 2007; revision received 4 October 2007; accepted for publication 28 October 2007. Copyright © 2007 by the American Institute of Aeronautics and Astronautics, Inc. All rights reserved. Copies of this paper may be made for personal or internal use, on condition that the copier pay the $10.00 per-copy fee to the Copyright Clearance Center, Inc., 222 Rosewood Drive, Danvers, MA 01923; include the code 0731-5090/08 $10.00 in correspondence with the CCC.

*Research Fellow, Department of Mechanical Engineering; thomas.waters@strath.ac.uk.

†Professor, Department of Mechanical Engineering; colin.mcinnes@strath.ac.uk. Member AIAA.

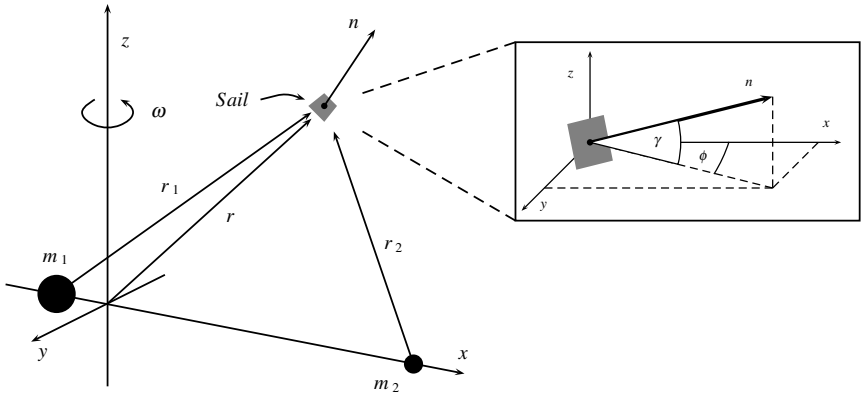

Fig. 1 Rotating coordinate frame, the sail position therein, and the angles γ and ϕ that the sail normal makes with respect to the rotating frame.

previously with the use of invariant manifolds. Invariant manifolds are well-known tools for finding low-cost transfers (see, for example, Gómez et al. [14] and Koon et al. [15]). An advantage to using invariant manifolds for transferring solar sails is that the sail orientation is fixed along the manifold, and thus we minimize the maneuvering demands on the sail. With this representative mission, we hope to demonstrate the robustness and flexibility of the controlled solar sail. Also, we note how orbits and transfers with solar sails are free; that is, there is no propellent needed for the life of the mission in addition to that required to insert the sail into its initial orbit.

We must emphasize at this point that the circular restricted three-body problem is an idealization of the true solar system dynamics of a solar sail. The Earth's orbit is, in fact, elliptical rather than circular, and other bodies in the solar system (for example, the moon, Jupiter, etc.) will perturb the sail's motion. The work presented in this paper is a first step in more fully examining the motion of a solar sail in the pure CR3BP, and therefore we will neglect the effects of perturbations due to ellipticity and other bodies.

Finally, in Sec. VI, we present some novel methods for finding periodic orbits based on considerations of the center manifold theorem and show how this is useful for cases when the traditional LP method breaks down (for example, at fixed points in the x–y–z space). In Sec. VII, we give some conclusions.

First, we briefly recap the important features of the fixed points in the solar sail CR3BP, as described in [5,16].

II. Background

We will follow the conventions set out in McInnes [16] and consider a rotating coordinate system in which the primary masses are fixed on the x axis with the origin at the center of mass. The z axis is the axis of rotation and the y axis completes the triad. We chose our units to set the gravitational constant, the sum of the primary masses, the distance between the primaries, and the magnitude of the angular velocity of the rotating frame to be unity; in this system, therefore, the unit of distance equals 1.496×10^8 km and the unit of velocity equals 29.8 km/s. We shall denote by $\mu = 3 \times 10^{-6}$ the dimensionless mass of the smaller body m_2, the Earth; therefore, the mass of the larger body m_1, the sun, is given by $1 - \mu$ (see Fig. 1).

Denoting by $\boldsymbol{r}$, $\boldsymbol{r}_1$, and $\boldsymbol{r}_2$ the position of the sail with regard to the origins m_1 and m_2, respectively, the solar sail's equations of motion in the rotating frame are [16]

$$\frac{\mathrm{d}^2\boldsymbol{r}}{\mathrm{d}t^2} + 2\boldsymbol{\omega} \times \frac{\mathrm{d}\boldsymbol{r}}{\mathrm{d}t} = \boldsymbol{a} - \boldsymbol{\omega} \times (\boldsymbol{\omega} \times \boldsymbol{r}) - \nabla V \equiv \boldsymbol{F} \tag{1}$$

with $\boldsymbol{\omega} = \hat{\boldsymbol{z}}$ and $V = -[(1-\mu)/r_1 + \mu/r_2]$, where $r_i = |\boldsymbol{r}_i|$. Letting $\boldsymbol{X} = (\boldsymbol{r}, \dot{\boldsymbol{r}})^T$, we can write the equations of motion as the first-order nonlinear system:

$$\dot{\boldsymbol{X}} = \boldsymbol{f}(\boldsymbol{X}; \boldsymbol{u}) \tag{2}$$

where $\boldsymbol{u}$ is the parameter set and a dot denotes differentiation with regard to time. These differ from the classical equations of motion in the CR3BP by the radiation pressure acceleration term [16]:

$$\boldsymbol{a} = \beta \frac{(1-\mu)}{r_1^2} (\hat{\boldsymbol{r}}_1 \cdot \boldsymbol{n})^2 \boldsymbol{n} \tag{3}$$

where β (the sail lightness number) is the dimensionless ratio of the solar radiation pressure acceleration to the solar gravitational acceleration. For the purpose of this paper, we are assuming an ideal (perfectly reflecting) sail, although generalizations to nonideal sails are straightforward [4].

Here, $\boldsymbol{n}$ is the unit normal of the sail and describes the sail's orientation. We define $\boldsymbol{n}$ in terms of two angles γ and ϕ with regard to the rotating coordinate frame:

$$\boldsymbol{n} = (\cos(\gamma)\cos(\phi), \cos(\gamma)\sin(\phi), \sin(\gamma))^T \tag{4}$$

where γ and ϕ are the angles the normal makes with the x–y and x–z plane, respectively (see Fig. 1). Throughout the paper, these angles will be given in radians.

Fixed points are given by the zeroes of $\boldsymbol{F}$ in Eq. (1), and we find a three-parameter family of the same specified by the triple (β, γ, ϕ), with each set of parameters defining two fixed points, one on the L_1 side of the Earth and one on the L_2 side (see Fig. 2). When $\gamma = 0$, fixed points are in the x–y plane, and when $\phi = 0$, fixed points are in the x–z plane. By linearizing system (1) about a fixed point and examining the linear system's eigenvalues, we find that fixed points in the x–z plane have the linear dynamic properties of centers crossed with saddles and have the linear spectrum

$$\{\pm\lambda_1 i, \pm\lambda_2 i, \pm\lambda_r\} \tag{5}$$

On the other hand, fixed points in the x–y–z space have the properties of stable/unstable spirals crossed with saddles. Because we are particularly interested in periodic orbits about fixed points built from the linear centers, we will therefore consider those fixed points in the x–z plane ($\phi = 0$) to be of primary interest; however, in Sec. VI, we will also discuss periodic orbits about fixed points outside of this plane.

The form of Eq. (5) tells us the structure of the invariant manifolds of nonlinear system (2), and we may conclude the following (we will drop the term *invariant*):

1) There is one stable and one unstable manifold associated with each fixed point, both of dimension one, and they characterize the flow onto and away from the fixed point.

2) There is a four-dimensional center manifold upon which trajectories oscillate about the fixed point with a combination of frequencies λ_1 and λ_2, in orbits that are a generalization of a set of classical curves known as *roses*. In particular, there are two two-dimensional foliations of the center manifold on which the frequencies separate; these paraboloidal surfaces contain the periodic orbits in each frequency λ_1 and λ_2.

The λ_1 family consists of roughly vertical orbits, and thus we will call them the halo type or $\mathcal{H}$ type; on the other hand, the λ_2 family is

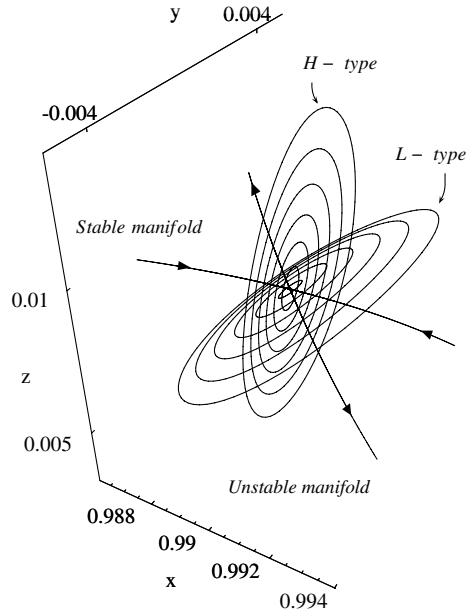

Fig. 2 Relevant parameters for fixed points in the x–z plane (negative z is not shown, due to symmetry in the x–y plane): β and γ level curves that specify the position of the fixed point (top), values of the linear frequencies λ_1 and λ_2 (bottom), positions at which the linear frequencies are in resonance with $\lambda_1 = 2\lambda_2$ (dashed line). In both, the position of the Earth, L_1, and L_2 are shown, with the fixed points going to L_1/L_2 in the limit $\beta \to 0$ or $\gamma \to \pi/2$. The shaded areas of the plot represent regions in which equilibrium is not possible.

made up of more horizontal orbits, and thus we will call them the Lyapunov type or $\mathcal{L}$ type (see Fig. 3). In [5], the authors described the $\mathcal{H}$-type family of periodic orbits, and in Sec. IV, we will describe the $\mathcal{L}$-type family.

These manifolds are useful because, in a sense, they summarize the dynamics associated with each parameter set, and they show an at-a-glance approximation to the general structure of solutions to nonlinear system (1). In Fig. 2, we show the important features of the fixed points in the x–z plane, as determined from the analysis in [5].

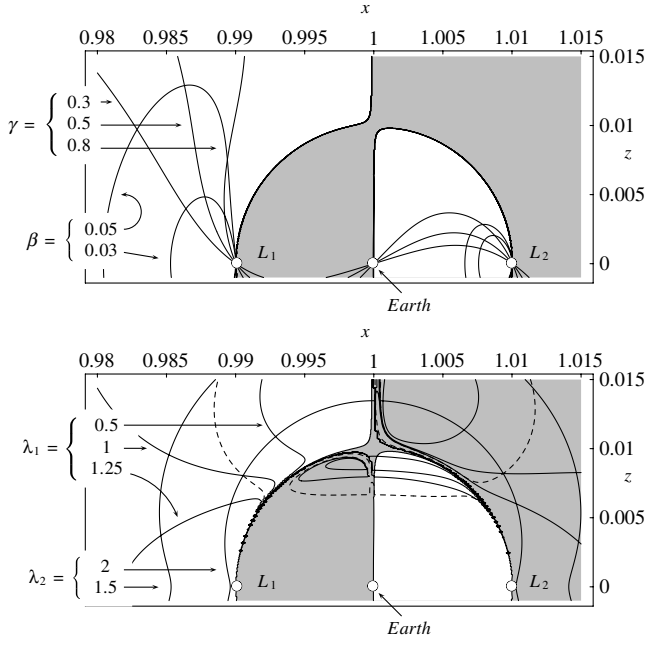

Fig. 3 Projections in configuration space of portions of the invariant manifolds associated with a typical fixed point in the x–z plane (in this case, the nominal point).

III. Optimal Control onto Fixed Points

Let the subscript e denote a value at an equilibrium or fixed point, such that $\boldsymbol{F}(\boldsymbol{r}_e) = 0$. Letting $\boldsymbol{r} \to \boldsymbol{r}_e + \delta\boldsymbol{r}$, where $\delta\boldsymbol{r} = (\delta x, \delta y, \delta z)^T$, we write the first-order linearized system as $\delta\dot{\boldsymbol{X}} = A \cdot \delta\boldsymbol{X}$, with

$$\delta\boldsymbol{X} = (\delta\boldsymbol{r}, \delta\dot{\boldsymbol{r}}), \qquad A = \begin{pmatrix} 0 & I \\ M & \Omega \end{pmatrix}$$
$$\Omega = \begin{pmatrix} 0 & 2 & 0 \\ -2 & 0 & 0 \\ 0 & 0 & 0 \end{pmatrix}, \qquad M_{ij} = \left.\frac{\partial \boldsymbol{F}_i}{\partial \boldsymbol{r}_j}\right|_e \tag{6}$$

As mentioned previously and shown in [5], A will admit at least one positive real eigenvalue, implying that the fixed point $\boldsymbol{r}_e$ is unstable.

The mechanism of control is to allow the angles γ and ϕ to vary. Some authors consider allowing β to vary; however, this is practically inefficient, and so we will discount it here. Letting $\boldsymbol{u} = (\gamma, \phi)^T \to \boldsymbol{u}_e + \delta\boldsymbol{u}$, our controller linear system becomes

$$\begin{aligned} \delta\dot{\boldsymbol{X}} &= A \cdot \delta\boldsymbol{X} + B \cdot \delta\boldsymbol{u} = A \cdot \delta\boldsymbol{X} + B(-G \cdot \delta\boldsymbol{X}) \\ &= (A - B \cdot G)\delta\boldsymbol{X} = A_c \cdot \delta\boldsymbol{X} \end{aligned} \tag{7}$$

where $A = \partial\boldsymbol{f}/\partial\boldsymbol{X}$ and $B = \partial\boldsymbol{f}/\partial\boldsymbol{u}$, and we have introduced the 2×6 gain matrix G via a feedback control law. We seek to define G such that the controlled linear system $\delta\dot{\boldsymbol{X}} = A_c \cdot \delta\boldsymbol{X}$ is asymptotically stable; that is, the eigenvalues of A_c all have negative real part.

Because this is a multivariable control system, it is overdefined, and so we may use the freedom to minimize the cost function:

$$J = \int (\delta\boldsymbol{X}^T \cdot Q \cdot \delta\boldsymbol{X} + \delta\boldsymbol{u}^T \cdot N \cdot \delta\boldsymbol{u})\, \mathrm{d}t \tag{8}$$

where Q and N are symmetric positive semidefinite and definite weighting matrices, respectively. By standard control systems theory [13], this is solved by $G = N^{-1}B^T P$, where the performance matrix P solves the algebraic Riccati equation:

$$A^T P + PA + Q - PBN^{-1}B^T P = 0 \tag{9}$$

There are a number of methods for solving this equation; however, the method we favor here consists of constructing the following Hamiltonian matrix:

$$H = \begin{pmatrix} A & -BN^{-1}B^T \\ -Q & -A^T \end{pmatrix} \tag{10}$$

A Hamiltonian matrix is any matrix of the form $(A, M_1), (M_2, -A^T)$, where M_1 and M_2 are symmetric, and has the property that if λ is an eigenvalue, then so is $-\lambda$, $\bar{\lambda}$, and $-\bar{\lambda}$. We compute the eigenvalues of H and take the first n as those with negative real part. For each of these stable eigenvalues, compute the eigenvectors v in $\mathbb{R}^{2n}$ and partition it as $v = (f_i, g_i)^T$ with $f_i, g_i \in \mathbb{R}^n$. Define the matrices $X_1 = (f_i)$ and $X_2 = (g_i)$, and let the performance matrix be $P = X_2 X_1^{-1}$. From this we calculate G, and this gives the optimally controlled system, according to the weights Q and N.

We are free to choose the weights themselves, Q and N, as long as they satisfy the properties mentioned previously. We will reduce this freedom to one parameter by letting $Q = I_6$ and $N = \rho I_2$ (although we note the possible advantages in weighting some elements of the diagonals over others). Thus, by varying ρ, we can choose whether the controller penalizes the control effort (ρ large) or the distance from equilibrium (ρ small), according to Eq. (8). Typically, when control onto a point or orbit is required, then ρ is set to be small, and in this section and in Secs. IV and V that follow, we will let $\rho = 10^{-4}$ unless stated otherwise. In Sec. VI, however, we will discuss some control strategies with ρ large.

With this gain matrix, we have forced the linearized controlled system to be asymptotically stable. Now we take this *linear* control scheme and use it to define the *nonlinear* controlled system as

$$\dot{\boldsymbol{X}} = \boldsymbol{f}(\boldsymbol{X}; \boldsymbol{u}_e + \delta\boldsymbol{u}) \tag{11}$$

In the vicinity of the fixed point the linear system dominates and trajectories are controlled; the question now reduces to the following: How far from the fixed point may we place the sail in phase space such that the resultant trajectory remains controlled? This is equivalent to asking how far the linear approximation extends in phase space.

This domain of controllability (DOC) in six-dimensional phase space will vary from one fixed point to the next and, remembering that there is a two-parameter family of fixed points in the x–z plane, this means that there is a very large space to search. To give a crude approximation to the DOC, we will therefore describe sets of initial data of increasing distance from the fixed point using spherical coordinates, and using these, we will integrate the controlled nonlinear system until one of two things happens: 1) the trajectory is not controlled and escapes from the vicinity of the fixed point or 2) the parameters γ and ϕ leave their allowed ranges:

$$-\pi/2 < \gamma, \qquad \phi < \pi/2 \tag{12}$$

This second condition is due to typical sail design of having only one reflective side, and thus we must have $\boldsymbol{n} \cdot \hat{\boldsymbol{r}}_1 > 0$.

We do not claim that this test presents a definitive measure of the domain of controllability for each fixed point; we merely claim that the tests can provide us with a first method of comparing the relative controllability of different fixed points, suggesting the directions in which the controller is most inefficient.

With this in mind, our first test will be to let the displacement from the fixed point be $\pm R$ in each coordinate direction in phase space; that is,

$$\delta\boldsymbol{X} = (\pm R, 0, 0, 0, 0, 0), \ldots, (0, 0, 0, 0, 0, \pm R)$$

and steadily increase R until we find a maximum value for each fixed point. Fixing β, this gives an $R_{\max} - \gamma$ plot, as shown in Fig. 4. We can make four observations from this quick test:

1) Fixed points on the L_1 side have a larger DOC than those on the L_2 side [this is because the L_2-side fixed points move closer to the Earth as β increases, which acts as a strong perturber in contrast with the L_1 side (see Fig. 2)].

2) The largest value of $R_{\max}$ occurs at the value of γ that gives the fixed point that is highest over the ecliptic plane: that is, the largest z_e.

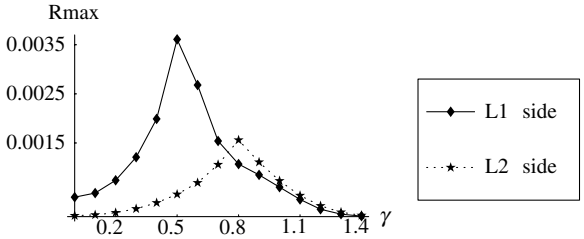

Fig. 4 Maximum values of R in each coordinate direction in phase space for fixed points along the $\beta = 0.05174$ level curve. The largest $R_{\max}$ occurs at $\gamma = 0.5$ and 0.8 for the L_1 and L_2 fixed points, respectively. The nominal fixed point $\gamma = 0.8092$ on the L_1 side is only moderately controllable.

3) This value of $R_{\max}$ can be surprisingly large (at best, 0.0035 in nondimensional units), which is equivalent to a positional displacement of 500, 000 km or a velocity displacement of 100 m/s.

4) From monitoring which trajectory first fails the test, we see that the controller is most sensitive to displacements in the x direction.

Based on the last point here, as a second test, we consider fixing $\delta x = 0$ and examining how large the displacements in the other directions may be. We separate the coordinate and velocity directions and set initial data as follows. The coordinate displacements are on a circle of radius R_1 in the δy–δz plane, and the velocity displacements are on a sphere of radius R_2 in the $\delta\dot{x}$–$\delta\dot{y}$–$\delta\dot{z}$ space. This leads to the displacement in phase space having magnitude $\sqrt{R_1^2 + R_2^2}$. To define the values of the initial data on the circle and sphere, we use polar/spherical coordinates as follows:

$$\begin{cases} \delta y = R_1 \cos(\theta_1), \quad \delta z = R_1 \sin(\theta_1), \\ \delta\dot{x} = R_2 \cos(\psi_2), \quad \delta\dot{y} = R_2 \sin(\psi_2)\cos(\theta_2), \quad \delta\dot{z} = R_2 \sin(\psi_2)\sin(\theta_2) \end{cases} \quad \text{with} \quad \begin{cases} 0 \le \theta_1, \theta_2 < 2\pi \\ 0 \le \psi_2 \le \pi \end{cases} \tag{13}$$

The position of the initial data value is determined by incrementing the angles θ_1 and (θ_2, ψ_2) by the fixed amounts Δ_1 and Δ_2, respectively. For example, when $\Delta_1 = \Delta_2 = \pi/2$, there are 4×6 distinct initial data points; however, when $\Delta_1 = \Delta_2 = \pi/4$, there are 8×26.

Using these sets of initial data, we integrate the controlled nonlinear system until the trajectory escapes or the sail tips over $\boldsymbol{n} \cdot \hat{\boldsymbol{r}}_1 > 0$. We find that we may increase R_1 and R_2 to quite large values and still maintain control onto the equilibrium point. For example, if $R_2 = R_1/10$, we may increase R_1 about the nominal fixed point ($\gamma_e = 0.8092$) up to a value of 0.0057 (see Fig. 5).

Finally, the natural question to ask is, Which direction is the most controllable? That is, with zero initial velocity, how large a positional displacement may there be and still maintain control? The answer is the $+z$ direction, in which we can control up to the order of $\delta z = 0.015$ (2 million km); this is quite remarkable, remembering that L_1 is only 0.01 (1.5 million km) away from the Earth (although this distance will be dwarfed by some of the orbits discussed in the next section).

IV. Optimal Control onto Periodic Orbits

In this section, we will use a simple discrete method to optimally control onto a periodic orbit. First, we choose the nominal orbit onto which we wish to control. We see from Eq. (5) that there are two families of periodic orbits about fixed points in the x–z plane, what we call $\mathcal{H}$ type and $\mathcal{L}$ type, and we show some of these orbits in Fig. 3 and their frequency values in Fig. 2. In [5], the authors describe a LP method to provide high-order approximations to periodic $\mathcal{H}$-type solutions to uncontrolled nonlinear system (2), and the same method applies to the $\mathcal{L}$-type family. A slight modification is to let the linear-order solution be

$$\begin{aligned} x_1 = kA_y \cos(\lambda_* t + \xi_*), \qquad y_1 = A_y \sin(\lambda_* t + \xi_*) \\ z_1 = mA_y \cos(\lambda_* t + \xi_*) \end{aligned} \tag{14}$$

where $\lambda_* = \lambda_1, \lambda_2$, depending on whether we wish to approximate the $\mathcal{H}$- or $\mathcal{L}$-type orbits, respectively; and k and m are coefficients made up of components of the eigenvectors. We have chosen to let the free parameter be the y amplitude A_y, because [due to the (assumed) symmetry in the x–z plane] two members of different families will only touch when their y amplitudes are the same. Also, members of the $\mathcal{H}$- and $\mathcal{L}$-type families may pass through vertically or horizontally, in which case, $A_x = 0$ or $A_z = 0$, respectively, which

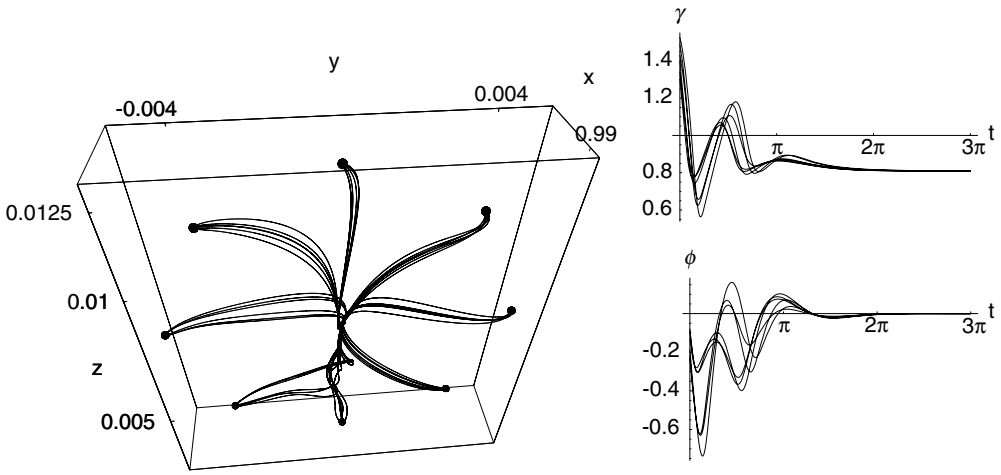

Fig. 5 Control to the nominal point given by $\beta = 0.05174$ and $\gamma_e = 0.8092$; set of trajectories found from initial data $R_1 = 10$ and $R_2 = 0.005$, although this goes up to 0.0057; $\Delta_1 = \pi/4$ and $\Delta_2 = \pi/2$. On the right is the largest control effort, from point $\theta_1 = 5\pi/4$; that is, the control effort from the six trajectories with varying velocity from the same position.

would lead to singular coefficients if these were chosen as free parameters. The LP method uses these linear solutions to build up approximations to periodic solutions to the nonlinear system in the following way. Let $\delta x = \varepsilon x_1 + \varepsilon^2 x_2 + \varepsilon^3 x_3 + \cdots$ etc., where

$$x_n = \sum_{j=0}^{n} A_j \cos[j(\lambda_* \omega t + \xi_*)] \tag{15}$$

and $\omega = 1 + \varepsilon\omega + 1 + \varepsilon^2\omega_2 + \cdots$. Then, using the free parameters ω_i to switch off the secular terms in the nth-order Taylor expansion of Eq. (2) about the fixed point, we solve a set of algebraic equations for the coefficients A_j (see [5] for a more detailed discussion).

The result is a trigonometric cosine and sine series parameterized by A_y in the (x, z) and y coordinates, respectively. We find it most convenient to use *these* analytic representations as nominal orbits to control onto, rather than the numerical orbits found from using a differential corrector to fine-tune initial data, for the following reasons:

1) The numerical orbits can only be found for amplitudes up to the limit of the approximations providing convergent initial data (without using numerical continuation, which is not really an option for a two-parameter family of fixed points); on the other hand, though the approximations do not provide convergent initial data, they do provide a close enough approximation to the orbit itself for the controller to control onto, even for large amplitudes.

2) These analytic representations are *exactly* periodic, rather than the almost-periodic numerical orbits.

The procedure is therefore straightforward: we split the nominal orbit into a series of points by incrementing the period, and at each point, we define the constant gain matrix using the same methods in Sec. III as if the point on the orbit were a fixed point. Then the components of the gain at each moment are interpolated to provide an approximation to a periodic gain. As with the fixed points, we find that this control method also works very well, and we propose a series of tests to measure the effectiveness of the control scheme. These tests are as follows:

1) Test 1: First we ask, How far from the initial data provided by the LP approximations may we be for the controller to bring us onto the nominal orbit?

2) Test 2: A sail placed at the fixed point can be controlled directly onto a periodic orbit using the periodic gain defined previously; from rest at the fixed point, onto how large of an amplitude orbit may we control the sail?

3) Test 3: Finally, beginning with the initial data provided by the LP approximations, how does the controller bring us onto a periodic orbit?

We will give the details of each test in turn.

1) The initial data point provided by the approximations is in the x–z plane (although we can easily choose somewhere else along the orbit); thus, we set the initial coordinates to be on a circle in the x–z plane centered on the nominal initial data position, and we set the velocities to be on the sphere centered on the nominal initial velocity, as in Eq. (13). With this setup, we integrate the periodically controlled nonlinear system until the trajectory escapes or the sail tips over ($\boldsymbol{n} \cdot \hat{\boldsymbol{r}}_1 > 0$). With this method, we can examine the controllability of the nominal periodic orbit; however, there is a four-parameter family of periodic orbits (two parameters specifying the fixed point and the two families $\mathcal{H}$ and $\mathcal{L}$ about that point), and so for the sake of brevity, we will not present an exhaustive search here. Instead, we will focus only on the nominal point ($\beta = 0.05174$ and $\gamma_e = 0.8092$). For $\mathcal{H}$-type orbits about this point, and letting $R = R_1 = R_2$, we find that as A_y increases from 0.001 to 0.005, the maximum value of R increases steadily from 0.0007 to 0.00085. On the other hand, $\mathcal{L}$-type orbits have a maximum R, increasing steadily from 0.00085 to 0.00115, all other things being equal.

2) This is a useful question with regard to transfer, as we shall see in Sec. V. We take $\boldsymbol{X} = (x_e, y_e, z_e, 0, 0, 0)^T$ as our initial data and integrate the controlled nonlinear system using the gain defined by a specified orbit of either $\mathcal{H}$ or $\mathcal{L}$ type with amplitude A_y. This gives the largest-amplitude orbit we may control onto from that fixed point, and in Fig. 6, we show the largest amplitude of each family for fixed points along the $\beta = 0.05174$ level curve. Control onto the $\mathcal{L}$-type

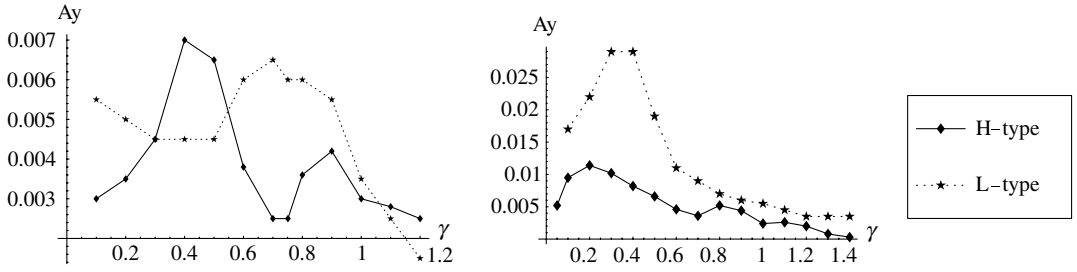

Fig. 6 Largest-amplitude orbits for members of the different families about fixed points on the $\beta = 0.05174$ curve on the L_1 side of the Earth. On the left is the control from the fixed point onto the orbit (test 2), and on the right is control from the initial data provided by the LP approximations (test 3).

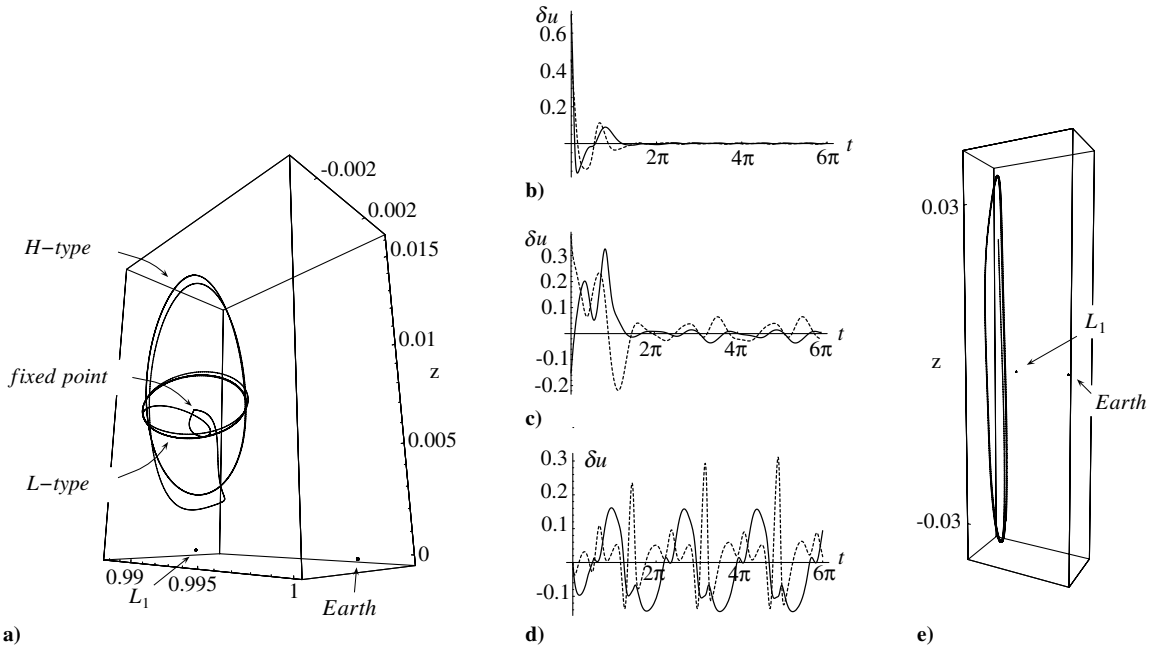

Fig. 7 Some examples of control onto periodic orbits: a) control onto $\mathcal{L}$- and $\mathcal{H}$-type orbits of amplitude $A_y = 0.0035$ from the nominal fixed points $\beta = 0.05174$ and $\gamma_e = 0.8092$ as in test 2, b) control effort for the $\mathcal{L}$-type orbits in part a, c) control effort for the $\mathcal{H}$-type orbits in part a, d) control effort for the control from the initial data onto an $\mathcal{H}$-type orbit with $A_y = 0.0052$ about $\beta = 0.05174$ and $\gamma_e = 0.05$ as in test 3, and e) the orbit itself. In parts b, c, and e, the solid line is $\delta\gamma = \gamma - \gamma_e$ and the dashed line is $\delta\phi$.

family is relatively unremarkable: the amplitude we may control onto hovers around the $A_y = 0.005$ mark mostly, with the orbits themselves being as expected. On the other hand, the $\mathcal{H}$-type family shows a large dip around the $\gamma = 0.7$ point, and this is due to a resonance effect: there is a fixed point along this β level curve ($\gamma = 0.751$) at which the linear frequencies satisfy $\lambda_1 = 2\lambda_2$ (see Fig. 2). When we try to control onto the $\mathcal{H}$-type orbit about this point, the orbits the sail controls onto become more egglike and develop a cusp at one end; passing through this cusp, a doubly periodic orbit emerges. We will not further discuss the nature of such orbits. We do not see this resonance in the $\mathcal{L}$-type orbits.

In Fig. 7a, we show an example of control onto periodic orbits from the fixed point. The orbits we may control onto have moderately large amplitudes and become prominent for large-amplitudes nonlinear effects; the orbits the control effort brings the sail onto become asymmetric and displaced from the nominal orbits of the LP approximation.

3) With this test, we see very large-amplitude orbits and, perhaps unsurprisingly, equally strong nonlinear effects. The amplitudes of the orbits the controller brings the sail onto have especially large amplitudes when γ is small, which corresponds to the sail facing onto the sun. Although the y amplitudes may look moderate, the orbit is elongated in the z direction and the resulting orbit can have a z amplitude on the order of 0.06 (10 million km)! This is really quite remarkable and is six times the distance of L_1 from the Earth (see Fig. 7e).

We can conclude that with regard to periodic orbits, the $\mathcal{L}$-type family are the more robust and that combined with a controller, the solar sail can be placed on large-amplitude periodic orbits of varying period, position, and inclination with small control effort.

V. Mission Strategies and Transfers

In previous sections, we attempted to give an overview of the effects of an optimal controller with regard to fixed points and periodic orbits. In this section, we will try to show how these methods can be used for a practical mission, and in the process, we hope to demonstrate the range and flexibility of the controlled solar sail.

The mission we have in mind consists of the following stages:

1) Transfer of the solar sail from the Earth's vicinity to the nominal fixed point ($\beta = 0.05174$ and $\gamma_e = 0.8092$) on the L_1 side of the Earth.

2) Moving from this fixed point onto a one-year orbit for an arbitrary time and then back to the fixed point.

3) Finally, transferring from a fixed point on the L_1 side to a fixed point on the L_2 side of the Earth with the same β value.

A possible application of this scenario is to facilitate transfer from the day side of the Earth to the night side for science missions, as well as the possible uses of high-elevation fixed points and one-year orbits already mentioned.

Transfer in the three-body problem is most efficiently achieved by taking advantage of the dynamics of the problem setting via the invariant manifolds. As mentioned in Sec. II, fixed points in the x–z plane will (without control) have one stable mode and one unstable mode due to a negative and positive real eigenvalue, respectively. Because the linear eigenspaces are tangential to the invariant manifolds at the fixed points, we can numerically approximate the stable/unstable manifolds by integrating system (2) in the direction of the stable/unstable linear eigenvectors either backward or forward in time. The solar sail three-body problem shares the y and z symmetries of the classical three-body problem; that is,

$$\{x, y, z, \dot{x}, \dot{y}, \dot{z}, t\} \rightarrow \{x, -y, z, -\dot{x}, \dot{y}, -\dot{z}, -t\} \tag{16}$$

$$\{x, y, z, \dot{x}, \dot{y}, \dot{z}, t\} \rightarrow \{x, y, -z, \dot{x}, \dot{y}, -\dot{z}, t\} \tag{17}$$

Thus, the stable manifold of a fixed point in the x–z plane is the image in the x–z plane under time reversal of the unstable manifold, and vice versa.

The practical use of these invariant manifolds is that if we can insert the sail onto the stable manifold of a fixed point in phase space, then the dynamics of the problem will naturally and freely carry the sail onto (or at least to the close vicinity of) the fixed point; also, if a sail is placed uncontrolled at a fixed point, the unstable manifold describes how the sail will fall away from the point and where it will naturally tend toward. What's more, transfers in which the sail orientation is fixed (that is, along invariant manifolds) will be easier to manage than those that require variations in the orientation.

In searching for a candidate trajectory for the first leg of the mission, we simply take a series of points along the β level curve of varying γ values and integrate Eq. (2) backward in time in the direction of the stable eigenvector; when we find one that passes close to the Earth, this is a candidate for transfer. In Fig. 8 we show

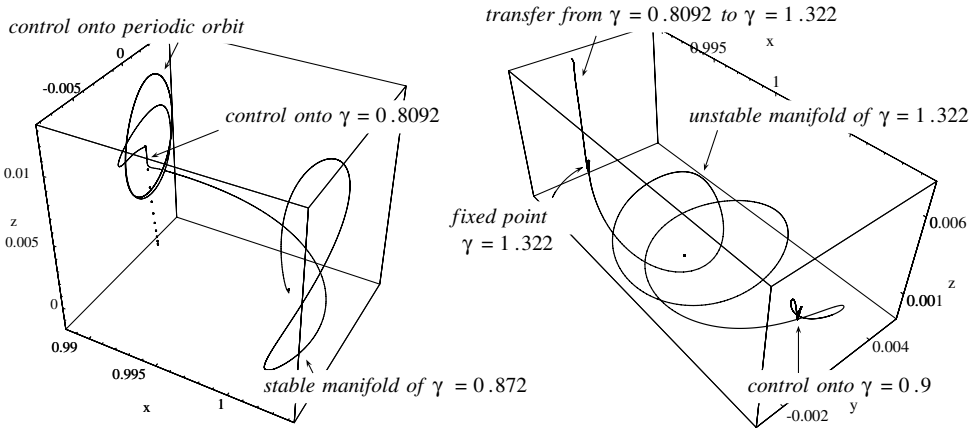

Fig. 8 The sample mission described in the text, with $\beta = 0.05174$ throughout. On the left is the transfer from the Earth along the stable manifold of the $\gamma = 0.872$ fixed point. When near the fixed point, the controller brings the sail onto the $\gamma = 0.8092$ point, as indicated. Then the controller brings the sail onto a periodic orbit about this point. On the right is the transfer from the $\gamma = 0.8092$ point to the $\gamma = 1.322$ point, then the controller is switched off and the sail falls away and into the vicinity of the L_2-side fixed points. There, the controller brings the sail onto the $\gamma = 0.9$ fixed point. The Earth is shown in both, and on the left is a series of dots representing the fixed points given by $\gamma = 0.8092, \ldots, \pi/2$.

how the stable invariant manifold of the fixed point ($\beta = 0.05174$ and $\gamma = 0.872$) passes close to the Earth and may be used for the transfer of the first leg. As the sail approaches the $\gamma = 0.872$ fixed point, the sail is controlled onto the $\gamma = 0.8092$ fixed point. The control effort for these two stages is shown in panels a and b of Fig. 9.

The second leg of the mission was discussed in Sec. IV. The nominal orbit about the nominal fixed point is of $\mathcal{H}$ type, with amplitude $A_y = 0.0026$ (as discussed in [5]), and we may control onto this orbit from the fixed point, because this amplitude is well within the acceptable range, as shown in Fig. 6. The trajectory is shown in Fig. 8. We note that if transfer to the orbit is the primary objective, it is easy to skip the intermediate stage of putting the sail at the fixed point and going directly onto the orbit by simply controlling from a point on the stable manifold of the $\gamma = 0.872$ fixed point onto the periodic orbit. Alternatively, trajectories in the stable invariant manifold of the periodic orbits that pass close to the Earth could be used, as mentioned in [5], although we will not pursue that option in this work. To return to the fixed point for the next stage is also typical, as discussed in Sec. III (by simply controlling onto the nominal fixed point from some point on the orbit). The control effort for these two stages is shown in panels c and d of Fig. 9.

The final leg consists of a transfer from a fixed point on the L_1 side to a fixed point on the L_2 side of the Earth. With regard to the stable/unstable invariant manifolds, there are two possible scenarios worth mentioning: homoclinic and heteroclinic paths. A homoclinic path joins an equilibrium point to itself; that, is the unstable manifold is identical to the stable manifold, and thus there is a trajectory that leaves the fixed point, only to return to it. A heteroclinic path is a

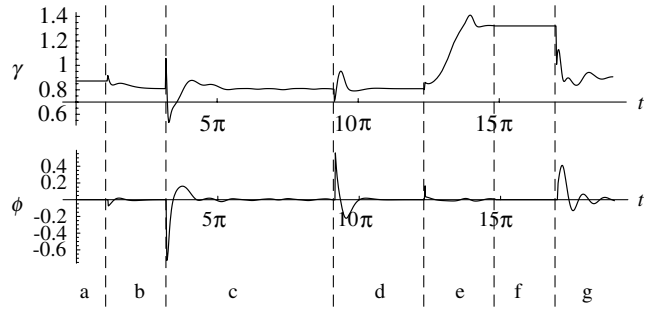

Fig. 9 The control effort required for the mission described in the text. Each leg of the mission is labeled as follows: a) transfer from Earth to $\gamma = 0.872$, b) control onto $\gamma = 0.8092$, c) control onto the periodic orbit, d) control back onto $\gamma = 0.8092$, e) control onto the $\gamma = 1.322$ fixed point, f) transfer to the L_2 side along the unstable manifold, and g) control onto the $\gamma = 0.9$ fixed point.

trajectory that joins two distinct equilibrium points; that is, the unstable manifold of one point smoothly meets the stable manifold of another. Note that these are asymptotic trajectories, and thus, for practical reasons, we must deal with their approximations by integrating system (1) in the direction of the linear eigenvectors.

Such paths are useful (particularly, the heteroclinic paths), because they essentially provide a free transfer: the dynamics of the three-body setting do all the work. As for their existence in the solar sail three-body problem, in a separate work [17], the authors displayed some homoclinic paths and, indeed, homoclinic invariant manifolds of periodic orbits in which each trajectory in a periodic orbit's invariant manifold is a homoclinic path. Heteroclinic paths are more difficult to come by, and we leave a systematic search for such features to a further work.

We use instead what we will call a controlled heteroclinic transfer, in which the unstable manifold of one fixed point passes close enough to another fixed point for the controller to finish the transfer. Finding candidate unstable manifolds is not as easy as it would at first appear, because (as already mentioned) a true heteroclinic path is an asymptotic one with the benefit that the sail will naturally slow down as it approaches the target fixed point. For nonheteroclinic paths, on the other hand, the sail will be moving quickly as it approaches the target and may be moving too quickly for the controller to work.

Instead, we look for an unstable invariant manifold that seems to be escaping from the Earth and then falls back toward the Earth in the vicinity of the β level curve on the far side; then the sail is moving slowly at this turning point and the controller has a better chance. We find that the $\gamma = 1.322$ fixed point has an unstable invariant manifold with this property; thus, we first need to bring the sail into the vicinity of this point. This is simply done by using the methods of Sec. III, and the control effort required is shown in panel e of Fig. 9. Then the controller is switched off and the sail is allowed to fall away on the unstable manifold, and thus γ is fixed (panel f of Fig. 9). When the sail is moving slowly in the vicinity of the L_2-side fixed points, the controller is switched on again to bring the sail onto the $\gamma = 0.9$ fixed point (panel g of Fig. 9). The trajectories for this third leg are shown in Fig. 8.

In general, the control effort over the length of the whole mission is relatively small; that is, γ and ϕ are largely fixed for most of the transfer. One of the drawbacks in using a solar sail for the missions outlined previously is the relatively long time scale, as is typical of solar sails, bearing in mind that 2π units in the nondimensionalized system represent one year. This, however, is a small price to pay, considering that there is no propellant consumption aside from that required to insert the sail onto its initial trajectory.

We note how the path of the sail may pass close to the Earth during transfer, and in this case, the effects of the Moon as a perturber of motion are important. The authors recognize that the next step in

examining transfers more accurately is to include the effects of the Moon. Because this means introducing a fourth body into the system, we leave this extension to further work.

VI. Alternative Routes to Periodic Orbits

In this final section, we present some alternative methods to finding periodic orbits using control. The first uses a large value of ρ, as given in Sec. III, and the second consists of using a single variable control scheme to assign eigenvalues based on the center manifold theorem.

As we described in Sec. III, an optimal controller minimizes a cost function according to arbitrary weighting matrices Q and N, as in Eq. (8). Letting $Q = I_6$ and $N = \rho I_2$ reduces the freedom of the weights to one parameter. Typically, when we wish to control to a fixed point without considering the control effort, we may set ρ to be small, and this is the procedure we have followed in this work so far ($\rho = 10^{-4}$). This strongly effects the eigenvalues of the controlled linear system A_c. If, on the other hand, we were to choose a large value of ρ, the controller would seek to minimize the control effort and not the distance from equilibrium, and thus the sail would orbit the fixed point rather than fall onto it (at least for moderate time scales).

We see this most clearly in the form the eigenvalues of A_c take for $\rho = 10^4$, for example. If the eigenvalues of A, the uncontrolled linear system, are

$$\{\pm\lambda_1 i, \pm\lambda_2 i, \pm\lambda_r\} \tag{18}$$

then the eigenvalues of A_c will be approximately

$$\{-\epsilon \pm \lambda_1 i, -\epsilon \pm \lambda_2 i, -\lambda_r, -\lambda_r\} \tag{19}$$

with ϵ small. This means that each mode is asymptotically stable; however, the real modes will decay and, because the real part of the complex modes is so small, the imaginary parts will dominate. Thus, the sail will orbit the fixed point according to the frequencies λ_1 and λ_2. As previously pointed out, if these frequencies are not in ratio, the sail will follow a dense rose-type orbit, akin to the Lissajous orbits about the classical collinear points. If the frequencies are in ratio, then the orbit will close, forming a possible multiply periodic orbit.

The advantage of this method is that the sail will orbit the fixed point for long times with a minimum of control effort. The sail may eventually fall onto the point, because the system is asymptotically stable, although weakly so. The orbit the sail follows is sensitive to the initial data and, depending on this, the sail will follow an orbit in one frequency of a mixture of the linear frequencies. Nonetheless, the center manifold of this controlled system will be close to the center manifold of the uncontrolled system, and so the orbits in it will be similar. In a way, this suggests the disadvantage of the optimal controller; that is, we cannot specify the eigenvalues of the controlled system directly, merely how strongly asymptotically stable they should be.

An alternative is to consider a single variable controller with which we may explicitly assign the eigenvalues of the controlled linear system. We will show how we may use this to describe periodic orbits in a direct way, but first, we will describe the method.

Choose a parameter u^* to vary, either γ or ϕ. Let $B = \partial \boldsymbol{f}/\partial u^*$; the controlled linear system is $A_c = A - B \cdot G$, where G is 1×6 now. Choose six eigenvalues λ_i and construct the desired characteristic polynomial $(\lambda - \lambda_1)\cdots(\lambda - \lambda_6)$. Form the characteristic polynomial of A_c in terms of the components of G, and equate the coefficients of these two polynomials. Then solve uniquely for the components of the gain G.

The natural question that follows is, What eigenvalues should we choose? We take some guidance from Eq. (19) and the center manifold theorem, which we can state in loose terms as the following:

Center Manifold Theorem: If the eigenvalues of a dynamic system linearized about a fixed point are stable (negative real part) and imaginary (zero real part), the stability or otherwise of the fixed point is determined by the system reduced to the center manifold.

What this essentially means is that the stable modes die out, and thus trajectories are, in a sense, pushed onto the center manifold. Once there, the stability of the fixed point may be determined by using normal forms to reduce the system to the center manifold. The benefit is that the dimension of the center manifold may be much smaller than that of the full system, greatly simplifying the analysis (see Carr [18] or Troger and Steindl [19] for a discussion).

We are not much interested in the stability of the fixed point, however, because we may freely specify it. Instead, the idea is that if we choose the linear eigenvalues to satisfy the theorem, then we should see the same behavior (i.e., trajectories being pushed onto the center manifold and remaining there). There are three distinct advantages to using this method:

1) Fixed points in the x–y–z space do not have center eigenvalues at linear order, and thus the LP method cannot be used directly to find approximations to periodic orbits. We note that one alternative is to perturb the dynamic system so that the linear system does contain centers, with the perturbation being picked up at higher order. This is just like the halo orbits about the classical collinear points, in which the linear system is perturbed to ensure that the in-plane and out-of-plane frequencies are the same. However, this becomes quite cumbersome; for example, when using a differential corrector, because the nice symmetry of the orbits about points in the x–z plane is lost.

Using the preceding methods, however, we can simply assign center eigenvalues at linear order using an appropriately chosen gain. We give an example of this later.

2) Not only can we assign the magnitude of the stable modes, but we may also assign the frequency of the center modes. This may be useful for specific missions: for example, the one-year orbits described in [5].

3) Assigning only one pair of center modes removes the difficulty of choosing initial data to fall onto the $\mathcal{H}$- or $\mathcal{L}$-type orbits, because there is only one family and it attracts all trajectories (in the vicinity of the fixed point).

For example, consider the fixed point

$$\begin{cases} \beta = 0.05, \quad \gamma_e = 0.5, \quad \phi_e = 0.095 \\ x_e = 0.98713, \quad y_e = 0.009855, \quad z_e = 0.0143 \end{cases} \tag{20}$$

Linearizing Eq. (2) about this point, we see that the linear eigenvalues are

$$\{-0.0047 \pm 1.319i, 0.025 \pm 0.768i, -0.548, 0.508\} \tag{21}$$

that is, a stable spiral, an unstable spiral, and a saddle (note that the saddle modes are not of equal magnitude because the symmetry of fixed points in the x–z plane is lost). As mentioned, there are no center eigenvalues to build up periodic orbits using the LP method. Instead, we assign the eigenvalues of the controlled linear system to be

$$\{\pm\lambda_c i, -\lambda_1, -\lambda_2, -\lambda_3, -\lambda_4\} \tag{22}$$

with λ_i real and positive. Then, the real stable modes will die out and the trajectory will fall onto the two-dimensional center manifold. For example, for the preceding fixed point, we will let the eigenvalues be

$$\{\pm 0.76i, -0.5, -1, -1.3, -1.5\}$$

which gives a gain of

$$(-115.3, 20.26, 5.53, -87.8, -18.4, -45.15)$$

We find that the controller works best when we assign the center frequency to be close to the imaginary part of one of the linear system's eigenvalues; which controller chosen distinguishes between the two families of orbits (although for small amplitudes, there is more freedom to let the frequency differ).

The disadvantage of this approach is that we are not specifying a nominal orbit to control onto; the initial data determine the amplitude

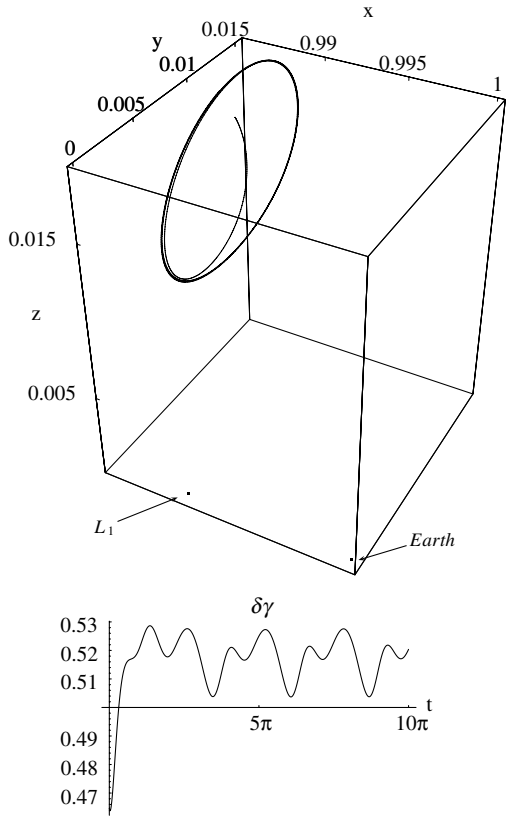

Fig. 10 A periodic orbit around the fixed point in the *x*–*y*–*z* space (described in the text) and the control effort. The Earth and L_1 are shown. In some cases, it is useful to put a small negative real part in front of the center eigenvalues (in this case, $-0.012 \pm 0.76i$).

of the orbit the controller brings the sail onto. Not surprisingly, therefore, this approach is sensitive to initial conditions. With a little experimentation, though, large-amplitude periodic orbits may be found about fixed points in the *x*–*y*–*z* space (see Fig. 10).

VII. Conclusions

We examined the control characteristics of solar sails in the Earth–sun circular restricted three-body problem (CR3BP). By first designing an optimal controller for fixed points, we showed that the sail may be controlled onto a fixed point from quite large displacements in phase space. Then, using a simple discrete method, we described the optimal control onto periodic orbits and showed that, again, the controller is very robust under a number of simple tests. To more fully demonstrate the capabilities of the controlled solar sail, we devised a sample mission involving transfer from the Earth and between fixed points; the analysis of this sample mission combined the use of invariant manifolds of fixed points with an optimal controller. Finally, we outlined some novel techniques for finding periodic orbits using the controller in situations in which the LP method breaks down. To conclude, the solar sail combined with an efficient controller can enable a whole variety of interesting and useful orbits in the CR3BP with minimum cost and effort.

Acknowledgment

This work was funded by grant EP/D003822/1 from the Engineering and Physical Sciences Research Council (EPSRC) of the United Kingdom.

References

[1] Dachwald, B., "Optimal Solar Sail Trajectories for Missions to the Outer Solar System," *Journal of Guidance, Control, and Dynamics*, Vol. 28, No. 6, 2005, pp. 1187–1193.

[2] McInnes, C., McDonald, M., Angelopolous, V., and Alexander, D., "GeoSail: Exploring the Geomagnetic Tail Using a Small Solar Sail," *Journal of Spacecraft and Rockets*, Vol. 38, No. 4, 2001, pp. 622–629.

[3] McInnes, C., McDonald, A., Simmons, J., and McDonald, E., "Solar Sail Parking in Restricted Three-Body Systems," *Journal of Guidance, Control, and Dynamics*, Vol. 17, No. 2, 1994, pp. 399–406.

[4] McInnes, C. R., "Artificial Lagrange Points for a Nonperfect Solar Sail," *Journal of Guidance, Control, and Dynamics*, Vol. 22, No. 1, 1999, pp. 185–187.

[5] Waters, T., and McInnes, C., "Periodic Orbits Above the Ecliptic in the Solar Sail Restricted 3-Body Problem," *Journal of Guidance, Control, and Dynamics*, Vol. 30, No. 3, 2007, pp. 687–693. doi:10.2514/1.26232

[6] Baoyin, H., and McInnes, C., "Solar Sail Halo Orbits at the Sun–Earth Artificial L_1 Point," *Celestial Mechanics and Dynamical Astronomy*, Vol. 94, No. 2, 2006, pp. 155–171. doi:10.1007/s10569-005-4626-3

[7] McInnes, A., "Strategies for Solar Sail Mission Design in the Circular Restricted Three-Body Problem," M.S. Thesis, Purdue Univ., West Lafayette, IN, 2000.

[8] Lawrence, D., and Piggott, S., "Solar Sailing Trajectory Control for Sub-L_1 Stationkeeping," AIAA Guidance, Navigation, and Control Conference and Exhibit, Providence, RI, AIAA Paper 2004-5014, 16–19 Aug. 2004.

[9] Baoyin, H., and McInnes, C., "Solar Sail Equilibria in the Elliptical Restricted Three-Body Problem," *Journal of Guidance, Control, and Dynamics*, Vol. 29, No. 3, 2006, pp. 538–543.

[10] Bookless, J., and McInnes, C., "Dynamics and Control of Displaced Periodic Orbits Using Solar Sail Propulsion," *Journal of Guidance, Control, and Dynamics*, Vol. 29, No. 3, 2006, pp. 527–537.

[11] McInnes, C., "Control for Displaced Solar Sail Orbits," *Journal of Guidance, Control, and Dynamics*, Vol. 21, No. 6, 1998, pp. 975–982.

[12] Gómez, G., Llibre, J., Martínez, R., and Simó, C., *Dynamics and Mission Design Near Libration Point Orbits*, Vol. 1, World Scientific, Singapore, 2001.

[13] Ogata, K., *Modern Control Engineering*, Prentice–Hall, Upper Saddle River, NJ, 2002.

[14] Gómez, G., Koon, W., Lo, M., Marsden, J., Masdemont, J., and Ross, S., "Invariant Manifolds, the Spatial Three-Body Problem and Petit Grand Tour of Jovian Moons," *Libration Point Orbits and Applications*, edited by G. Gómez, M. W. Lo, and J. Masdemont, World Scientific, Singapore, 2003.

[15] Koon, W., Lo, M., Marsden, J., and Ross, S., "Heteroclinic Connections Between Periodic Orbits and Resonance Transitions in Celestial Mechanics," *Chaos*, Vol. 10, June 2000, pp. 427–469. doi:10.1063/1.166509

[16] McInnes, C. R., *Solar Sailing: Technology, Dynamics and Mission Applications*, Springer Praxis, London, 1999.

[17] Waters, T., and McInnes, C., "Solar Sail Dynamics in the Three-Body Problem: Homoclinic Paths of Points and Orbits," *International Journal of Non-Linear Mechanics* (submitted for publication).

[18] Carr, J., *Applications of Centre Manifold Theory*, Springer–Verlag, New York, 1981.

[19] Troger, H., and Steindl, A., *Nonlinear Stability and Bifurcation Theory*, Springer–Verlag, New York, 1991.